Extended Abstracts of the 2012 International Conference on Solid State Devices and Materials, Kyoto, 2012, pp837-838

Random Telegraph Signals under External Mechanical Stress: A New Method to Probe Trap Structural Relaxation in MOSFET Gate Dielectrics

Kong-Chiang Tu and Ming-Jer Chen
Department of Electronics Engineering, National Chiao-Tung University, Hsinchu, Taiwan;
E-mail: chenmj@faculty.nctu.edu.tw

1. Abstract

For the first time, we present the characterization and analysis of random telegraph signals (RTS) in MOSFETs undergoing an externally applied tensile stress. All the energetic criteria involved in the trapping/de-trapping kinetics are shown to increase with stress: the trap level in gate oxide, the thermal activation energy for electron capture, and the atomic-displacement relaxation energy as the strength of electron-lattice coupling. These together lead to the unambiguous determination of the configuration coordinate diagrams of individual gate dielectric traps.

2. Introduction

Recently, performing MOSFET RTS measurements has been increasingly important. The essential reasons are that the measured capture and emission time constants contain the information about the configuration coordinate diagrams of the individual traps in gate dielectrics [1]-[3] (see Fig. 1). The merits of the configuration coordinate context are that (i) it can provide a phenomenological description of both the atomic-displacement structural relaxation and the electron-lattice coupling; and (ii) straightforwardly, it can have potential applications in the areas of bias temperature instability [4] and carrier transport through high-k stacks [5]. However, there was one unsolved issue to date: which of these two diagrams in Fig. 1 is practically responsible for the observed RTS?

On the other hand, external mechanical stress has been employed in the study of strain-altered channel mobility and gate tunneling current [6]. However, MOSFET RTS measurements were not yet done under external stress.

In this work, external mechanical stress is, for the first time, incorporated while performing MOSFET RTS characterization and analysis. As a consequence, responsible configuration coordinate diagrams are unambiguously determined.

3. Experimental

Two n-channel MOSFETs were presented: Trap A with W/L=0.15/0.5um and Trap B with W/L=0.12/0.1um. The key process parameters were obtained by C-V fit, as depicted in Fig. 2. A four-point mechanical bending system was established, as in Fig. 3. The external tensile stress was fixed at 200 MPa. The drain voltage was set to 0.02 V for all measurements at 297 K. Fig. 4 shows measured I_d and I_g versus V_g before and after stress. Corresponding stress-induced changes in I_d and I_g at V_g = 1 V agree with literature values [6], confirming the external stress experiment in this work. Fig. 5 shows the evolution of I_d over a long period of time. Two-level fluctuations due to the pre-existing oxide traps are evident. Corresponding capture time τ_c and emission time τ_e follow exponential distribution, as shown in Fig. 6. Fitted mean capture time $<\tau_c>$ and mean emission time $<\tau_e>$ before and after stress are plotted in Fig. 7 versus Vg. The figure shows that $<\tau_c>$ increases but $<\tau_e>$ decreases as stress is applied. Corresponding $<\tau_c>/<\tau_e>$ increases with stress, as in Fig. 8.

4. Analysis and Discussion

First, we employed a self-consistent Schrödinger and Poisson's equations solver [7], with the aforementioned process parameters and stress value as inputs. The outcomes contain the Fermi level E_f, inversion-layer electron density N_s, inversion-layer quantum thickness z_{qm}, and lowest subband level E_o, as well as Coulomb energy ΔE [8] via a capacitive coupling equivalent circuit [2]. ΔE is a function of the trap depth in oxide, z_t [2]. The principle of dynamic balance, taking into account ΔE [8], was used to extract z_t and the trap level E_t:

$$\frac{\tau_c}{\tau_e} = e^{\frac{(E_t - E_f + \Delta E)}{k_B T}} \quad (1)$$

Fitting results are illustrated in Fig. 8. Extracted E_t increases with stress. Corresponding ΔE exhibits a decreasing trend with stress, as displayed in Fig. 9. The thermal activation energy E_B was further assessed by following the expression with ΔE included [8]:

$$\frac{1}{\tau_c} = \sigma_o e^{-\frac{E_B}{k_B T}} v_{th} \frac{N_s}{z_{qm}} e^{-\frac{\Delta E}{k_B T}} \quad (2)$$

where v_{th} (= 1.23×10^5 m/s [2]) is the thermal velocity and σ_0 is the capture-cross-section pre-factor. Extracted E_B with $\sigma_0 = 1\text{x}10^{-18}$ cm^2 are shown in Fig. 10 versus Vg. The figure reveals an increasing trend of E_B with the stress. With known E_B, the $S\hbar\omega$ with two distinct values (one being small and another much larger, as separately demonstrated in Fig. 1), can be obtained by solving the equation [9]:

$$E_B = \frac{(E_o - E_t - S\hbar\omega)^2}{4S\hbar\omega} \quad (3)$$

Consequently, we reach the unambiguous determination of the configuration coordinate diagrams of underlying traps. The two samples feature a large $S\hbar\omega$; that is, case 1 in Fig. 1, as fully illustrated in Fig. 11. Corresponding trap parameters are listed in Table 1. Finally, we want to stress that the uncertainty in σ_0 does not affect the arguments in this work. To clarify this, $S\hbar\omega$ was re-extracted for varying σ_0, as in Fig. 12. Evidently, the change in relaxation energy is weak relative to σ_0 changed by orders of magnitude.

5. Conclusion

RTS measurements on external tensile stress nMOSFETs have been carried out. Sophisticated analyses have been conducted. Configuration coordinate diagrams of underlying traps have been created and have been identified. The presented work may enhance the current understanding of the configuration coordinate diagrams as well as their promising applications.

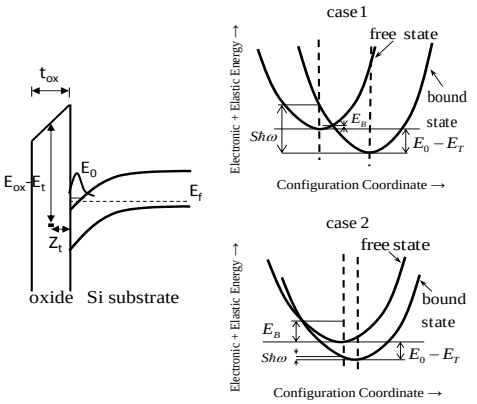

Fig. 1 Schematic illustration of the two distinct configuration coordinate diagrams for a gate-oxide trap.

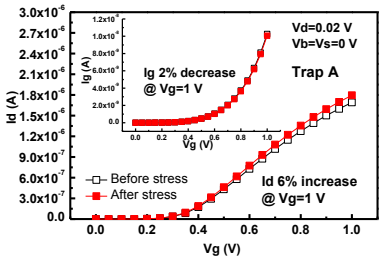

Fig. 4 Measured Id and Ig before and after stress.

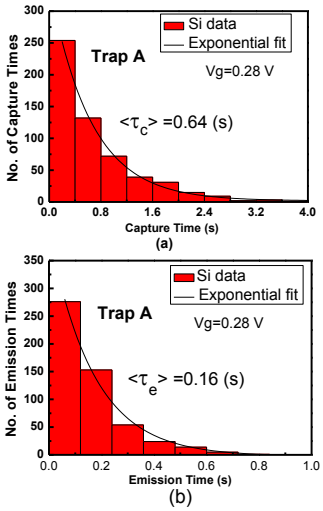

Fig. 6 Histograms of measured (a) capture time constant and (b) emission time constant. Exponential fit produces mean time constants.

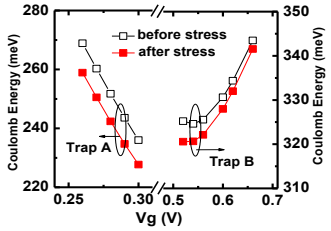

Fig. 9 Coulomb energy versus gate voltage before and after stress

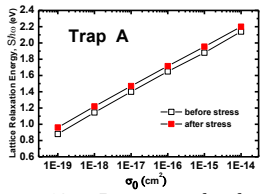

Fig. 12 Re-extracted lattice relaxation energy versus capture cross section pre-factor before and after stress.

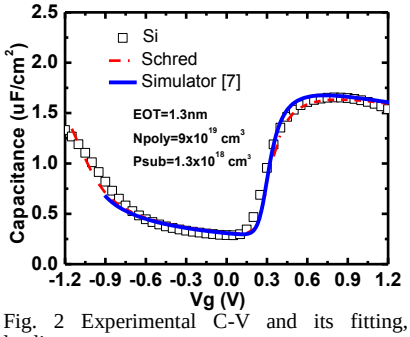

Fig. 2 Experimental C-V and its fitting, leading to process parameters.

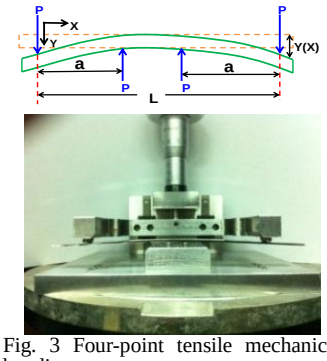

Fig. 3 Four-point tensile mechanical bending system

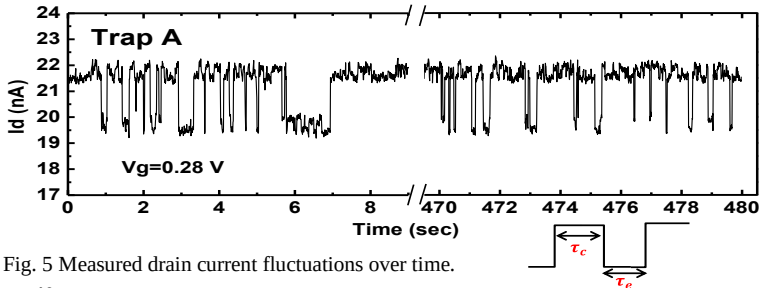

Fig. 5 Measured drain current fluctuations over time.

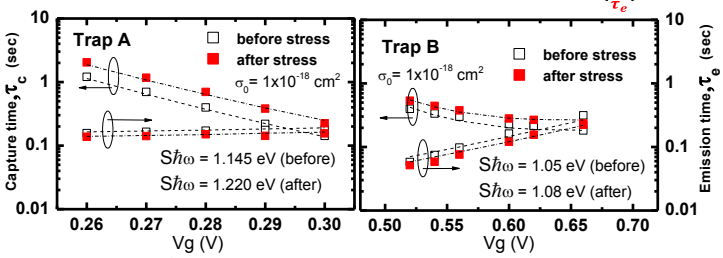

Fig. 7 Comparison of experimental (symbols) and calculated (lines) mean capture time constants and emission time constants versus gate voltage before and after stress.

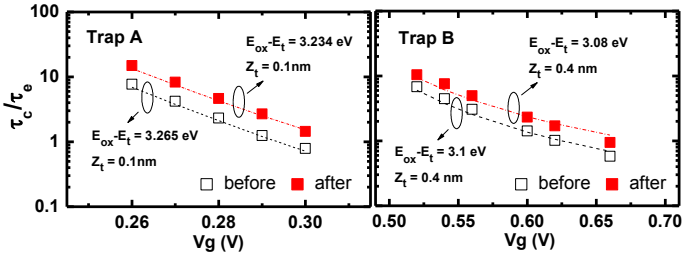

Fig. 8 Comparison of experimental (symbols) and calculated (lines) mean capture to emission time ratio versus gate voltage before and after stress.

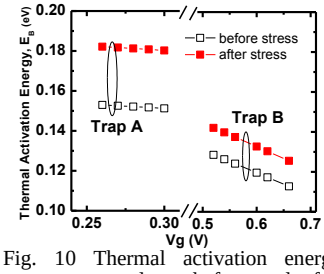

Fig. 10 Thermal activation energy versus gate voltage before and after stress.

	Z_t (nm)		E_{ox}-E_t (eV)		Sħω (eV)		E_B (eV)
	before	after	before	after	before	after	after
Trap A	0.1	0.1	3.265	3.234	1.145	1.22	↑
Trap B	0.4	0.4	3.1	3.08	1.05	1.08	↑

Table 1 Extracted trap parameters for both samples.

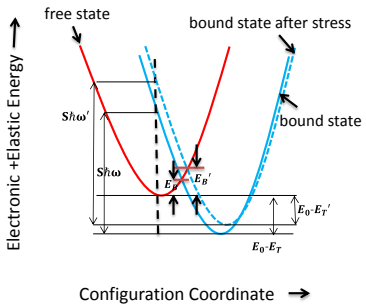

Fig. 11 Identified configuration coordinate diagrams before and after stress, valid for both Trap A and Trap B.

Acknowledgement

This work was supported by the National Science Council of Taiwan under Contract No. NSC 100-2221-E-009-017-MY3.

References

[1] M. J. Kirton and M. J. Uren, *Adv. Phys. 38*, p. 367, 1989. [2] M. P. Lu and M. J. Chen, *Phys. Rev. B, 72*, p. 235417, 2005. [3] D. Veksler, et al., *IRPS*, 2010, p.73. [4] T. Grasser, et al., *IEDM*, 2009, p. 729. [5] L. Vandelli, et al., *IEEE TED*, 9, p. 2878, 2011. [6] S. E. Thompson, et al., *IEEE TED*, 5, p.1010, 2006. [7] M. J. Chen and W. H. Lee, *IEEE EDL*, 6, p. 755, 2012. [8] M. Schulz, *JAP*, 74, p. 2649, 1993. [9] C. H. Henry and D. V. Lang, *Phys. Rev. B*, 15, p. 989, 1977.